Optimal Mixing Enhancement in 3-D Pipe Flow

Andras Balogh, Ole Morten Aamo, *Member, IEEE*, and Miroslav Krstić, *Fellow, IEEE*

***Abstract*—We design a Lyapunov based-boundary feedback controller for achieving mixing in a three-dimensional (3-D) pipe flow governed by Navier–Stokes equations. We show that the control law maximizes a measure related to mixing (that incorporates stretching and folding of material elements), while at the same time minimizing the control effort and the sensing effort. The penalty on sensing results in a static *output*-feedback control law (rather than full-state feedback). We also derive a lower bound on the gain from the control effort to the mixing measure. Furthermore, we establish input–output-to-state-stability properties for the open-loop system. These results show a form of detectability of mixing in the interior of the pipe from the chosen outputs on the wall. The effectiveness of the optimal control in achieving mixing enhancement is demonstrated in numerical simulations.**

***Index Terms*—Lyapunov methods, mixing, optimality, output feedback, partial differential equations.**

I. Introduction

THE PROCESS of mixing is encountered frequently in engineering applications, with the mixing of air and fuel in combustion engines being a prime example [8], [3]. Approaches to analyzing mixing range from experimental design and testing to modern applications of dynamical systems theory (see [24], [25] for thorough reviews). The latter was initiated by Aref [4], and followed by [5], [13], [17], [31], and [28]. A framework in which to analyze mixing properties of (nonperiodic) finite-time flow fields, was developed in [9]–[12], and applied to geophysical flows in [22] and [27]. Another method for identifying regions in a flow that have similar finite-time statistical properties based on ergodic theory was developed and applied in [19]–[20]. The relationship between the two methods mentioned, focusing on geometrical and statistical properties of particle motion, respectively, was examined in [26]. Rigorous application of control systems theory to problems in mixing appeared for the first time in [6] and [7], and more recently in [23]. For a more elaborate review of these works, see [1].

In [1], we applied active feedback control in order to enhance existing instability mechanisms in a two-dimensional (2-D) model of plane channel flow. By applying boundary control intelligently in a feedback loop, mixing was considerably enhanced with relatively small control effort. Wall-normal suction and blowing was used for actuation, and the pressure difference between opposite points on the wall for sensing. The control law was decentralized and designed using Lyapunov stability analysis.

In the current work, these efforts are successfully extended to three-dimensional (3-D) pipe flow, which, in the uncontrolled case, has a parabolic steady-state solution (known as Hagen–Poiseuille flow). With mixing in mind, we quantify the flow perturbations (away from the Hagen–Poiseuille flow) in terms of the L_2 norm of their first-order spatial derivatives. This norm is a volume integral over the entire flow domain. It explicitly incorporates stretching of material elements, and due to the boundedness of the domain, and the fact that the flow field satisfies the Navier–Stokes equations, folding is implicit in the measure. Since stretching and folding are key ingredients in mixing, the measure appears to be strongly related to mixing.

We design a Lyapunov based control law and show that it maximizes the measure of mixing described above, while at the same time minimizing the control effort and the sensing effort. The penalty on sensing results in a static *output*-feedback control law (rather than full-state feedback). We also derive a lower bound on the gain from the control effort to the mixing measure.

In separate results, we establish input–output-to-state-stability properties for the open-loop system. These results show a form of detectability of mixing in the interior of the pipe from the chosen outputs on the wall.

The effectiveness of the optimal control in achieving mixing enhancement is demonstrated in numerical simulations of the full, nonlinear, Navier–Stokes equations for 3-D pipe flow at Reynolds numbers 10, 2100, and 5000. To quantify mixing, massless particles are placed into the flow, simulating passive tracer dye. Visualizations compare perturbation energy, enstrophy, vorticity, and dye distribution for the uncontrolled and controlled cases.

The feedback system designed in this work stands a good chance of being realizable, due to its simplicity: sensing and actuation are restricted to the pipe wall; and the feedback law is decentralized and static. Furthermore, simulations show that the spatial changes in the control velocity are smooth and small, promising that a low number of actuators will suffice in practice.

This paper is organized as follows. In Section II, we present the governing equations. In Section III, we introduce our choices of sensing and actuation. In Section IV, we define two measures of the fluid flow field which are instrumental to the theoretical analysis. In Section V, we provide an energy analysis resulting in two technical lemmas that are frequently used in the analysis. In Section VI, we present the main result on control design and optimality. In Section VII, we discuss detectability of mixing. In Section VIII, numerical simulations are presented, and finally, in Section IX, we offer some concluding remarks.

Manuscript received September 5, 2003. Manuscript received in final form April 7, 2004. Recommended by Associate Editor A. Banaszuk. This work was supported by the Office of Naval Research, the Air Force Office of Scientific Research, the National Science Foundation, the Norwegian Research Council, and the Gas Technology Center at NTNU.

A. Balogh is with the Department of Mathematics, University of Texas-Pan American, Edinburg, TX 78541-2999 USA (e-mail: abalogh@panam.edu).

O. M. Aamo is with the Department of Engineering Cybernetics, Norwegian University of Science and Technology, N-7491 Trondheim, Norway (e-mail: aamo@itk.ntnu.no).

M. Krstić is with the Department of Mechanical and Aerospace Engineering, University of California at San Diego, La Jolla, CA 92093 USA (e-mail: krstic@ucsd.edu).

Digital Object Identifier 10.1109/TCST.2004.838544

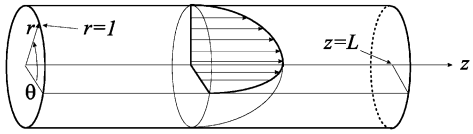

Fig. 1. Geometry of the pipe flow.

II. Navier–Stokes Equations for 3-D Pipe Flow

The nondimensionalized Navier–Stokes equation is given by

$$\frac{\partial \mathbf{W}}{\partial t} + (\mathbf{W}\cdot\nabla)\mathbf{W} = -\nabla P + \frac{1}{\mathrm{Re}}\Delta\mathbf{W} \tag{1}$$

$$\mathrm{div}(\mathbf{W}) = 0 \tag{2}$$

where ∇ denotes the gradient operator, Δ denotes the Laplace operator, and div is short for divergence. $\mathbf{W} : \Omega \times \mathbb{R}_+ \to \mathbb{R}^3$ is the velocity of the fluid, $P : \Omega \times \mathbb{R}_+ \to \mathbb{R}$ is the pressure, and Re is the Reynolds number. The Reynolds number is defined as $\mathrm{Re} = \rho\breve{D}\breve{V}/\mu$, where ρ and μ are the density and viscosity of the fluid, respectively, and $\breve{D}$ and $\breve{V}$ are characteristic length and characteristic velocity of the problem. The pipe radius is chosen as characteristic length, and the center velocity of the steady flow (Hagen–Poiseuille flow, given by (3) below) is chosen as characteristic velocity. The domain, Ω, for the 3-D pipe flow is most easily defined in terms of cylindrical coordinates (r,θ,z), configured as shown in Fig. 1. The domain is, thus, given by $\Omega = \{(r,\theta,z) \in [0,1)\times[0,2\pi)\times[0,L)\}$, where L is the length of the pipe. In the angular (θ) direction, the boundary conditions are clearly periodic. In the streamwise (z) direction, we also use periodic boundary conditions. That is, we equate the flow quantities at $\theta = 0$ and $\theta = 2\pi$, and at $z = 0$ and $z = L$. In the radial direction (r) we impose the boundary conditions that the velocity be finite at $r = 0$, and at the wall $(r = 1)$ we will eventually specify the flow velocity as a boundary control law, but for now we use no slip. Under these boundary conditions, one may verify that the velocity field, $\bar{\mathbf{W}}$, and pressure $\bar{P}$, defined by

$$(\bar{\mathbf{W}},\bar{P}) = (\bar{V}_r,\bar{V}_\theta,\bar{V}_z,\bar{P}) = \left(0,0,1-r^2,-\frac{4}{\mathrm{Re}}z\right) \tag{3}$$

is a steady-state solution of (1)–(2), where $\bar{V}_r$, $\bar{V}_\theta$, and $\bar{V}_z$ are the velocity components in the radial (r), angular (θ), and streamwise (z) directions, respectively. Equations (1)–(2) in terms of perturbation variables, defined as

$$\mathbf{w} \triangleq \mathbf{W} - \bar{\mathbf{W}} \quad \text{and} \quad p \triangleq P - \bar{P} \tag{4}$$

becomes

$$\frac{\partial \mathbf{w}}{\partial t} + (\bar{\mathbf{W}}\cdot\nabla)\mathbf{w} + (\mathbf{w}\cdot\nabla)\bar{\mathbf{W}} + (\mathbf{w}\cdot\nabla)\mathbf{w} = -\nabla p + \frac{1}{\mathrm{Re}}\Delta\mathbf{w} \tag{5}$$

$$\mathrm{div}(\mathbf{w}) = 0. \tag{6}$$

In cylindrical coordinates, we will denote the perturbation variables

$$\mathbf{w} = (v_r, v_\theta, v_z) \triangleq (V_r, V_\theta, V_z - \bar{V}_z), \quad \text{and} \quad p \triangleq P - \bar{P}. \tag{7}$$

We will frequently need volume integrals over the domain Ω, as well as area integrals over the boundary, which we denote

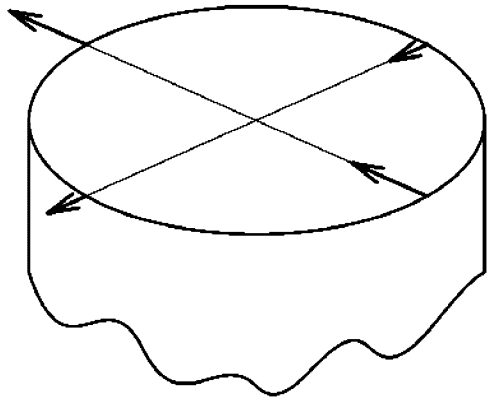

Fig. 2. Actuation is symmetric about the pipe centerline.

$\partial\Omega$. In view of the periodic boundary conditions in the angular and streamwise directions, the boundary is simply the pipe wall, $\partial\Omega = \{(r,\theta,z) : r = 1\}$. The volume and area integrals are denoted in the usual manner as

$$\int_\Omega (\cdot)\, dV \quad \text{and} \quad \int_{\partial\Omega} (\cdot)\, dA \tag{8}$$

respectively. The equivalent integrals in cylindrical coordinates are

$$\int_0^L \int_0^{2\pi} \int_0^1 (\cdot) r\, dr\, d\theta\, dz \quad \text{and} \quad \int_0^L \int_0^{2\pi} (\cdot) d\theta\, dz. \tag{9}$$

III. Sensing and Actuation

As mentioned in the previous section, the boundary conditions on the wall of the pipe incorporate our actuation. The fluid velocity at the wall is restricted to be normal to the wall, that is, $v_r(1,\theta,z,t) = u(\theta,z,t)$, and $v_\theta(1,\theta,z,t) = v_z(1,\theta,z,t) = 0$, where $u(\theta,z,t)$ is the control input. Thus, $\mathbf{w}\cdot\mathbf{n} = u$ on $\partial\Omega$, where $\mathbf{n}$ is the outward pointing unit normal vector. We also impose on the control input that it satisfies

$$u(\theta,z,t) = -u(\theta+\pi,z,t) \tag{10}$$

which states that if suction is applied at a point (θ,z) on the pipe wall, then an equal amount of blowing is applied at the opposite point $(\theta+\pi,z)$. This is illustrated in Fig. 2. It is clear that condition (10) ensures a zero net mass flux across the pipe wall, and therefore it is a natural condition to impose from a mass balance point of view. The measurement available is the pressure drop, denoted y, from any point (θ,z) on the pipe wall to the opposite point $(\theta+\pi,z)$. That is

$$y(\theta,z,t) \triangleq p(1,\theta,z,t) - p(1,\theta+\pi,z,t). \tag{11}$$

We also define the instantaneous control effort and sensing effort as

$$U(t) = \int_{\partial\Omega} u^2\, dA \tag{12}$$

and

$$Y(t) = \int_{\partial\Omega} y^2\, dA \tag{13}$$

respectively.

IV. Measures of Mixing

There are two key ingredients to effective mixing. The fluid flow field must inflict extensive stretching to material elements, and the stretching should be accompanied by folding. In this paper, we define two measures of the fluid flow field that are instrumental to our development below. One is the kinetic energy of the perturbation, termed *turbulent kinetic energy* in the fluid mechanics literature, defined as

$$E(\mathbf{w}) \triangleq \frac{1}{2}\int_{\Omega} |\mathbf{w}|^2\, dV = \frac{1}{2}\int_0^L \int_0^{2\pi} \int_0^1 \left(v_r^2 + v_\theta^2 + v_z^2\right) r\, dr\, d\theta\, dz \tag{14}$$

and the other is a measure of spatial velocity gradients, defined as

$$\begin{aligned} m(\mathbf{w}) &\triangleq \int_{\Omega} |\nabla \mathbf{w}|^2\, dV = \int_{\Omega} \mathrm{Tr}\left\{\nabla \mathbf{w}^T \nabla \mathbf{w}\right\} dV \\ &= \int_0^L \int_0^{2\pi} \int_0^1 \left[\left(\frac{\partial v_r}{\partial z}\right)^2 + \left(\frac{\partial v_\theta}{\partial z}\right)^2 + \left(\frac{\partial v_z}{\partial r}\right)^2 \right. \\ &\quad + \left(\frac{1}{r}\frac{\partial v_z}{\partial \theta}\right)^2 + \left(\frac{\partial v_z}{\partial z}\right)^2 + \left(\frac{\partial v_r}{\partial r}\right)^2 + \left(\frac{\partial v_\theta}{\partial r}\right)^2 \\ &\quad \left. + \left(\frac{v_r}{r} + \frac{1}{r}\frac{\partial v_\theta}{\partial \theta}\right)^2 + \left(\frac{v_\theta}{r} - \frac{1}{r}\frac{\partial v_r}{\partial \theta}\right)^2 \right] r\, dr\, d\theta\, dz. \end{aligned} \tag{15}$$

The latter measure (15), which is related to the *dissipation function* via the factor $1/\mathrm{Re}$, appears to be stronger connected to mixing. While it is clear that stretching of material elements is explicit in a measure of spatial gradients of the flow field, folding is implicit in the measure due to the boundedness of the flow domain, and the fact that $\mathbf{w}$ satisfies the Navier–Stokes equations. It is recognized that flow fields having poor mixing properties and large $m(\mathbf{w})$ exist, but we postulate that such flow fields will not be hydrodynamically stable under the control actuation to be designed below. Thus, our objective becomes that of designing a feedback control law, in terms of suction and blowing of fluid normally to the pipe wall that is optimal with respect to some meaningful cost functional related to $m(\mathbf{w})$.

V. Energy Analysis

Before giving the main result on controller design and optimality, we state two key lemmas that are needed frequently in what follows. The first lemma is a Lyapunov type result and it relates the time derivative of $E(\mathbf{w}(t))$ to $m(\mathbf{w}(t))$. The second lemma provides a bound on the crossterm between the perturbation and the Hagen–Poiseuille steady state flow, originating from the nonlinear convective terms in the Navier–Stokes equation. This term is called the *instantaneous production* in the fluid mechanics literature. Proofs of the lemmas are provided in Appendix.

Lemma 1 (Balance for the Turbulent Kinetic Energy): For wall-normal actuation, satisfying (10)

$$\dot{E}(\mathbf{w}) = -\frac{1}{2}\int_{\partial\Omega} uydA - \frac{1}{\mathrm{Re}}U - \frac{1}{\mathrm{Re}}m(\mathbf{w}) - \Gamma(\mathbf{w}) \tag{16}$$

along solutions of system (5)–(6), where

$$\Gamma(\mathbf{w}) = \int_{\Omega} [(\mathbf{w}\cdot\nabla)\bar{\mathbf{W}} + (\bar{\mathbf{W}}\cdot\nabla)\mathbf{w}]\cdot\mathbf{w}\, dV. \tag{17}$$

Lemma 2 (Bound for the Instantaneous Production): If $v_z(1,\theta,z,t) = 0$, then solutions of system (5)–(6) satisfy

$$\Gamma(\mathbf{w}) \le \frac{a}{2}(1+b)U + \max\left\{\frac{a}{4}\left(1+\frac{1}{b}\right), \frac{1}{4a}\right\} m(\mathbf{w}) \tag{18}$$

for arbitrary positive constants a and b.

The conditions of Lemma 1 and 2 are assumed to hold throughout the analysis that follows. That is, actuation is wall-normal and satisfies (10).

VI. Optimality

The following theorem incorporates the control design and optimality result.

Theorem 3: The control

$$u = -ky \tag{19}$$

with $k \in (0, \mathrm{Re}/4)$ and Re arbitrary, maximizes the cost functional

$$J(u) = \lim_{t\to\infty}\left[2\beta E(\mathbf{w}(t)) + \int_0^t h(\mathbf{w}(\tau))\, d\tau\right] \tag{20}$$

where

$$\beta = \frac{2k}{\left(1 - \frac{4}{\mathrm{Re}}k\right)}$$

and

$$h(\mathbf{w}) = \frac{2\beta}{\mathrm{Re}}m(\mathbf{w}) + 2\beta\Gamma(\mathbf{w}) - \left(\frac{\beta}{2}\right)^2\left(1+\frac{2\beta}{\mathrm{Re}}\right)^{-1} Y - U. \tag{21}$$

Moreover, the solutions of system (5)–(6) satisfy

$$h(\mathbf{w}) \le c_1 m(\mathbf{w}) - c_2 Y - \frac{1}{2}U \tag{22}$$

for arbitrary values of the control u, and with

$$c_1 = \frac{2\beta}{\mathrm{Re}} + \max\left(\frac{1}{4}, 2\beta^2\right) > 0 \tag{23}$$

and

$$c_2 = \left(\frac{\beta}{2}\right)^2\left(1+\frac{2\beta}{\mathrm{Re}}\right)^{-1} > 0. \tag{24}$$

Proof: By Lemma 1, we can write (21) as

$$h(\mathbf{w}) = -2\beta\dot{E}(\mathbf{w}) - \beta\int_{\partial\Omega} uydA - \frac{2\beta}{\mathrm{Re}}U - \left(\frac{\beta}{2}\right)^2\left(1+\frac{2\beta}{\mathrm{Re}}\right)^{-1} Y - U. \tag{25}$$

Inserting (25) into (20), we get

$$\begin{aligned}J(u) &= \lim_{t\to\infty}\left[2\beta E(\mathbf{w}(t)) + \int_0^t \left(-2\beta\dot{E}(\mathbf{w}(\tau))\right.\right.\\ &\quad -\beta\int_{\partial\Omega} uy\,dA - \left(1+\frac{2\beta}{\mathrm{Re}}\right)U\\ &\quad \left.\left. -\left(\frac{\beta}{2}\right)^2\left(1+\frac{2\beta}{\mathrm{Re}}\right)^{-1}Y\right)d\tau\right]\\ &= \lim_{t\to\infty}\left[2\beta E(\mathbf{w}(t)) - 2\beta\int_0^t \dot{E}(\mathbf{w}(\tau))\,d\tau\right.\\ &\quad -\left(1+\frac{2\beta}{\mathrm{Re}}\right)\int_0^t\int_{\partial\Omega}\left(u^2+\beta\left(1+\frac{2\beta}{\mathrm{Re}}\right)^{-1}uy\right.\\ &\quad \left.\left.+\left(\frac{\beta}{2}\right)^2\left(1+\frac{2\beta}{\mathrm{Re}}\right)^{-2}y^2\right)dA\,d\tau\right]\\ &= 2\beta E(\mathbf{w}(0)) - \left(1+\frac{2\beta}{\mathrm{Re}}\right)\lim_{t\to\infty}\int_0^t\int_{\partial\Omega}\left(u+\frac{\beta}{2}\right.\\ &\quad \left.\times\left(1+\frac{2\beta}{\mathrm{Re}}\right)^{-1}y\right)^2 dA\,d\tau. \end{aligned} \tag{26}$$

The maximum of (20) is achieved when the integral in (26) is zero. Thus, (19) is the optimal control. Inequality (22) is obtained by applying Lemma 2 with $a = (1/4\beta)$ and $b = 1$, to (21). ■

The objective of applying the control input (19) is to increase the value of $m(\mathbf{w})$. That this objective is targeted in the cost functional (20), is clear from inequality (22), which gives an upper bound on $h(\mathbf{w})$ in terms of $m(\mathbf{w})$. Thus, $h(\mathbf{w})$ cannot be made large without making $m(\mathbf{w})$ large, so the cost functional (20) is meaningful with respect to our objective. The cost functional also puts penalty on the output. Since the output is fed back to the control input, the output penalty works in conjunction with the input penalty to minimize control effort.

The next theorem writes the result of Theorem 3 on a form that puts emphasis on signal gains.

Theorem 4: For all Re and $t \geq 0$, solutions of system (5)–(6) satisfy

$$\max_{\substack{u\\ e(0)\neq 0}}\left\{\lim_{t\to\infty}\frac{e(t)+\int_0^t g(\mathbf{w}(\tau))\,d\tau}{e(0)+\int_0^t b(\mathbf{w}(\tau))\,d\tau}\right\} = 1 \tag{27}$$

where

$$e(t) \triangleq 2\beta E(\mathbf{w}(t)) \tag{28}$$

$$g(\mathbf{w}) \triangleq h(\mathbf{w}) + c_2 Y + \frac{1}{2}U \tag{29}$$

$$b(\mathbf{w}) \triangleq c_2 Y + \frac{1}{2}U \tag{30}$$

and

$$g(\mathbf{w}) \leq c_1 m(\mathbf{w}). \tag{31}$$

Furthermore, the maximum is achieved with the optimal control (19), for which solutions of the closed-loop system satisfy

$$\begin{aligned}&2\beta E(\mathbf{w}(t)) + c_1\int_0^t m(\mathbf{w}(\tau))\,d\tau\\ &\qquad \geq 2\beta E(\mathbf{w}(0)) + \left(\frac{3}{2}+\frac{2\beta}{\mathrm{Re}}\right)\int_0^t U(\tau)\,d\tau.\end{aligned} \tag{32}$$

Proof: Integration of (29) with respect to time, and adding $e(t)$ to each side, gives

$$\begin{aligned}&e(t) + \int_0^t g(\mathbf{w}(\tau))\,d\tau\\ &\qquad = e(t) + \int_0^t h(\mathbf{w}(\tau))\,d\tau + \int_0^t b(\mathbf{w}(\tau))\,d\tau.\end{aligned} \tag{33}$$

The two first terms on the right hand side of (33) is $J(u)$ (without the limit), so inserting (26) we get

$$\begin{aligned}e(t) + \int_0^t g(\mathbf{w}(\tau))\,d\tau &= e(0)\\ &\quad -\left(1+\frac{2\beta}{\mathrm{Re}}\right)\int_0^t\int_{\partial\Omega}\left(u+\frac{\beta}{2}\left(1+\frac{2\beta}{\mathrm{Re}}\right)^{-1}y\right)^2 dA\,d\tau\\ &\quad +\int_0^t b(\mathbf{w}(\tau))\,d\tau.\end{aligned} \tag{34}$$

Dividing both sides of (34) by

$$e(0) + \int_0^t b(\mathbf{w}(\tau))\,d\tau$$

assuming $e(0) \neq 0$, taking the limit as $t \to \infty$, and then taking the maximum value over u, we obtain

$$\begin{aligned}&\max_{\substack{u\\ e(0)\neq 0}}\left\{\lim_{t\to\infty}\frac{e(t)+\int_0^t g(\mathbf{w}(\tau))\,d\tau}{e(0)+\int_0^t b(\mathbf{w}(\tau))d\tau}\right\}\\ &\qquad = \max_{\substack{u\\ e(0)\neq 0}}\left\{1 - \lim_{t\to\infty}\frac{\gamma\int_0^t\int_{\partial\Omega}\left(u+\frac{\beta}{2\gamma}y\right)^2 dA\,d\tau}{e(0)+\int_0^t b(\mathbf{w}(\tau))\,d\tau}\right\}\end{aligned} \tag{35}$$

where

$$\gamma = \left(1+\frac{2\beta}{\mathrm{Re}}\right). \tag{36}$$

Since the numerator of the last term in (35) is nonnegative, and the denominator is strictly positive, the maximum on the right hand side of (35) is attained when the numerator is zero, which

is for the optimal control (19). Thus, we obtain (27). Inequality (31) follows from (29) and (22). Inserting the optimal control into (34) by writing y in terms of u using (19), we obtain

$$2\beta E(\mathbf{w}(t)) + \int_0^t g(\mathbf{w}(\tau))\,d\tau = 2\beta E(\mathbf{w}(0)) + c_2\left(\frac{2}{\beta}\right)^2\left(1+\frac{2\beta}{\mathrm{Re}}\right)^2\int_0^t U(\tau)\,d\tau + \frac{1}{2}\int_0^t U(\tau)\,d\tau. \quad (37)$$

Inserting for c_2, as defined in (24), and using (31), we get (32). ■

The result (27) was inspired by the work on optimal destabilization of linear systems reported in [21]. In view of (31), by maximizing the ratio in the curly brackets of (27), we make sure that the input and output signals are small compared to the internal states. This is equivalent to obtaining a large closed-loop gain. In addition, the theorem gives a lower bound on the states in terms of the control input for system (5)–(6) in closed loop with (19). Thus, it establishes the fact that the states cannot be small without the control input being small, and the control input cannot be made large without making the states large. As we shall see in our simulation study, this will lead to good mixing with low control effort.

VII. Detectability of Mixing

Achieving optimality with static output feedback of y is remarkable. In this section, we explain why this special output is strongly related to mixing and allows its enhancement. The next theorem establishes an open-loop property of system (5)–(6) that is reminiscent of an integral variant of input–output-to-state-stability (IOSS) for finite dimensional nonlinear systems.

Theorem 5: If $\mathrm{Re} \in (0,4)$, then solutions of system (5)–(6) satisfy

$$c_3\int_0^t m(\mathbf{w}(\tau))\,d\tau \le 2\beta E(\mathbf{w}(0)) + \beta^2\left(1+\frac{2\beta}{\mathrm{Re}}\right)^{-1}\int_0^t Y(\tau)\,d\tau + c_4\int_0^t U(\tau)\,d\tau \quad (38)$$

for all $t \ge 0$ and for arbitrary values of the control u, with

$$c_3 = \frac{\beta}{4}\left(\frac{4-\mathrm{Re}}{\mathrm{Re}}\right) > 0 \quad \text{and} \quad c_4 = 1+\beta\left(\frac{4+\mathrm{Re}}{4-\mathrm{Re}}\right) > 0.$$

Proof: From (20), (21), and (26), we get for all $t \ge 0$

$$2\beta E(\mathbf{w}(t)) + \int_0^t \frac{2\beta}{\mathrm{Re}} m(\mathbf{w}(\tau))\,d\tau \le 2\beta E(\mathbf{w}(0)) - 2\beta\int_0^t \Gamma(\mathbf{w}(\tau))\,d\tau + \left(\frac{\beta}{2}\right)^2\left(1+\frac{2\beta}{\mathrm{Re}}\right)^{-1}\int_0^t Y(\tau)d\tau + \int_0^t U(\tau)d\tau. \quad (39)$$

Using Lemma 2, we obtain

$$\begin{aligned}2\beta E(\mathbf{w}(t)) + \int_0^t \frac{2\beta}{\mathrm{Re}} m(\mathbf{w}(\tau))\,d\tau &\le 2\beta E(\mathbf{w}(0)) + 2\beta\int_0^t \left(\frac{a}{2}(1+b)U(\tau) + \max\left\{\frac{a}{4}\left(1+\frac{1}{b}\right), \frac{1}{4a}\right\} m(\mathbf{w}(\tau))\right)d\tau \\ &\quad + \left(\frac{\beta}{2}\right)^2\left(1+\frac{2\beta}{\mathrm{Re}}\right)^{-1}\int_0^t Y(\tau)\,d\tau + \int_0^t U(\tau)\,d\tau\end{aligned}$$

so it follows that:

$$\begin{aligned}2\beta E(\mathbf{w}(t)) + \int_0^t \frac{2\beta}{\mathrm{Re}} m(\mathbf{w}(\tau))\,d\tau &\le 2\beta E(\mathbf{w}(0)) + \int_0^t \frac{\beta}{2}\max\left(a\left(1+\frac{1}{b}\right), \frac{1}{a}\right) m(\mathbf{w}(\tau))\,d\tau \\ &\quad + \left(\frac{\beta}{2}\right)^2\left(1+\frac{2\beta}{\mathrm{Re}}\right)^{-1}\int_0^t Y(\tau)\,d\tau \\ &\quad + (1+\beta a(1+b))\int_0^t U(\tau)\,d\tau.\end{aligned}$$

Rearranging the terms, we obtain

$$\begin{aligned}&2\beta E(\mathbf{w}(t)) + \left(\frac{2\beta}{\mathrm{Re}} - \frac{\beta}{2}\max\left(a\left(1+\frac{1}{b}\right), \frac{1}{a}\right)\right)\int_0^t m(\mathbf{w}(\tau))\,d\tau \\ &\le 2\beta E(\mathbf{w}(0)) + \left(\frac{\beta}{2}\right)^2\left(1+\frac{2\beta}{\mathrm{Re}}\right)^{-1}\int_0^t Y(\tau)\,d\tau + (1+\beta a(1+b))\int_0^t U(\tau)\,d\tau\end{aligned}$$

which is (38) for $a = 1$ and $b = 2(\mathrm{Re})/(4-\mathrm{Re})$. ■

The significance of inequality (38) is that it provides a notion of detectability of internal states from the output y. In particular, if $m(\mathbf{w})$ is large, y must be large as well, or if y is small, so is $m(\mathbf{w})$. This is reminiscent of an integral variant of the IOSS property for finite-dimensional nonlinear systems, as presented in [15] (and motivated by earlier results in [29], [30]). In the case of (38), we have an integral-to-integral property (iiIOSS) with $m(\mathbf{w})$ as a measure of the states, so the "energy" of the states is bounded above by the "energy" of the input and output signals. With $E(\mathbf{w})$ as a measure of the states, we can also find a uniform upper bound (as opposed to an "energy" upper bound) in terms of the input and output signals. That is, system (5)–(6) has the IOSS property, as stated formally in the next theorem.

Theorem 6: For $\mathrm{Re} \in (0,4)$, solutions of system (5)–(6) satisfy

$$E(\mathbf{w}(t)) \le E(\mathbf{w}(0))e^{-c_5 t} + \frac{1}{4c_5}\sup_{\tau\in[0,t]} Y(\tau) + \frac{c_6}{c_5}\sup_{\tau\in[0,t]} U(\tau) \quad (40)$$

for all $t \ge 0$ and for arbitrary values of the control u, with

$$c_5 = 2\max\left(\frac{4}{3\mathrm{Re}} - 1, \frac{4-\mathrm{Re}}{4+\mathrm{Re}}\right) > 0$$

and

$$c_6 = \max\left(\frac{1}{4}, \frac{1}{4} + \frac{5\mathrm{Re}-4}{\mathrm{Re}(4-\mathrm{Re})}\right) > 0.$$

Proof: From (67), (68) and a similar derivation for v_θ, we have

$$2E(\mathbf{w}) \le \frac{1}{2}(1+b)U + \frac{1}{4}\int_0^L\int_0^{2\pi}\int_0^1 \left(\left(1+\frac{1}{b}\right)\left(\frac{\partial v_r}{\partial r}\right)^2 + \left(\frac{\partial v_\theta}{\partial r}\right)^2 + \left(\frac{\partial v_z}{\partial r}\right)^2\right) r\,dr\,d\theta\,dz \quad (41)$$

and therefore

$$2E(\mathbf{w}) \le \frac{1}{2}(1+b)U + \frac{1}{4}\left(1+\frac{1}{b}\right)m(\mathbf{w}). \quad (42)$$

From Lemma 1 and (42) we get

$$\dot{E}(\mathbf{w}) \le -2\left(\frac{4}{\mathrm{Re}}\left(\frac{b}{1+b}\right) - 1\right)E(\mathbf{w}) - \frac{1}{2}\int_{\partial\Omega} uy\,dA + \frac{2b-1}{\mathrm{Re}}U$$

so that

$$\dot{E}(\mathbf{w}) \le -2\left(\frac{4}{\mathrm{Re}}\left(\frac{b}{1+b}\right) - 1\right)E(\mathbf{w}) + \frac{1}{4}\int_{\partial\Omega}\left(u^2+y^2\right)dA + \frac{2b-1}{\mathrm{Re}}U.$$

Setting

$$b = \max\left(\frac{1}{2}, \frac{2\mathrm{Re}}{4-\mathrm{Re}}\right)$$

we obtain

$$\dot{E}(\mathbf{w}) \le -c_5 E(\mathbf{w}) + \frac{1}{4}Y + c_6 U \quad (43)$$

with

$$c_5 = 2\max\left(\frac{4}{3\mathrm{Re}} - 1, \frac{4-\mathrm{Re}}{4+\mathrm{Re}}\right)$$

and

$$c_6 = \max\left(\frac{1}{4}, \frac{1}{4} + \frac{5\mathrm{Re}-4}{\mathrm{Re}(4-\mathrm{Re})}\right).$$

Inequality (40) now follows from the comparison principle ([16], Lemma C.5) [and the triangle inequality applied to the two last terms in (43)]. ■

In Theorem 6, the notation $\sup_{[0,t]}$ denotes the essential supremum taken over the finite time interval $[0,t]$. The detectability properties stated in Theorems 5 and 6 indicate that our choice of sensing, y, is appropriate.

VIII. Numerical Simulations

A. Computational Scheme

The simulations are performed using a flow solver that is based on a second-order staggered grid discretization, second-order time advancement, and a Poisson equation for pressure, based on a scheme designed by Akselvoll and P. Moin [2]. The length of the cylinder is $L = 3\pi$ and the radius is $R = 1$. The grid is structured, single-block with cylindrical coordinates. It is uniform and periodic in z and θ with Fourier-modes 64 and 128, respectively, and linearly spaced with ratio 8:1 in the radial direction in order to achieve high resolution at the wall. The adaptive time step was in the range of 0.01–0.08 with constant CFL number 0.5 and constant 1 volume flux per unit span. Numerical results corresponding to three different Reynolds numbers are presented here. The lowest Reynolds number is $\mathrm{Re} = 10$ which is a stable, and perhaps nonphysical flow, but it is a good test case for the effectiveness of the control design. The second Reynolds number we used was $\mathrm{Re} = 2100$ which is slightly higher than the limiting number $\mathrm{Re} = 2000$ for self-sustained turbulence. Finally for the case of $\mathrm{Re} = 5000$ we compare natural and controlled turbulence.

We started both the controlled and the uncontrolled case from a statistically steady-state flow field with control gain $k = 0.1$ in the controlled case. The initial flow field was obtained from a random perturbation of the parabolic profile over a large time interval using the uncontrolled case. All the measured quantities were scaled to unit surface or unit volume, whichever was appropriate.

B. Measuring Mixing

We start our comparison with the spatially averaged perturbation energy and enstrophy defined as

$$\frac{1}{2V}\int_\Omega |\mathbf{w}|^2\,dV \quad \text{and} \quad \frac{1}{2V}\int_\Omega |\nabla\times\mathbf{w}|^2\,dV \quad (44)$$

respectively, where V denotes the volume of region Ω. While the perturbation energy is part of the cost functional (20) and is also one of the simplest quantities to measure in our numerical simulation, enstrophy provides us with a measurement that is more closely related to mixing. Fig. 3 shows that in the $\mathrm{Re} = 2100$ case our control results in an approximately 25% increase in the perturbation energy and 65% almost instantaneous increase in the perturbation enstrophy. For the $\mathrm{Re} = 5000$ case these numbers are smaller: approximately 15% and 40%, respectively. One sees the largest control effect in the $\mathrm{Re} = 10$ case: "infinite" % increase in the perturbation energy and enstrophy. Intuitively these differences are easy to understand. In a laminar flow ($\mathrm{Re} = 10$), there is no mixing, hence, this case can be dramatically improved with control. The $\mathrm{Re} = 2100$ case corresponds to self-sustained turbulence already, but it is not far from the laminar ($\mathrm{Re} = 2000$) case. In this border case, it is expected that our control can easily tip the scale toward increased turbulence and mixing. In the fully

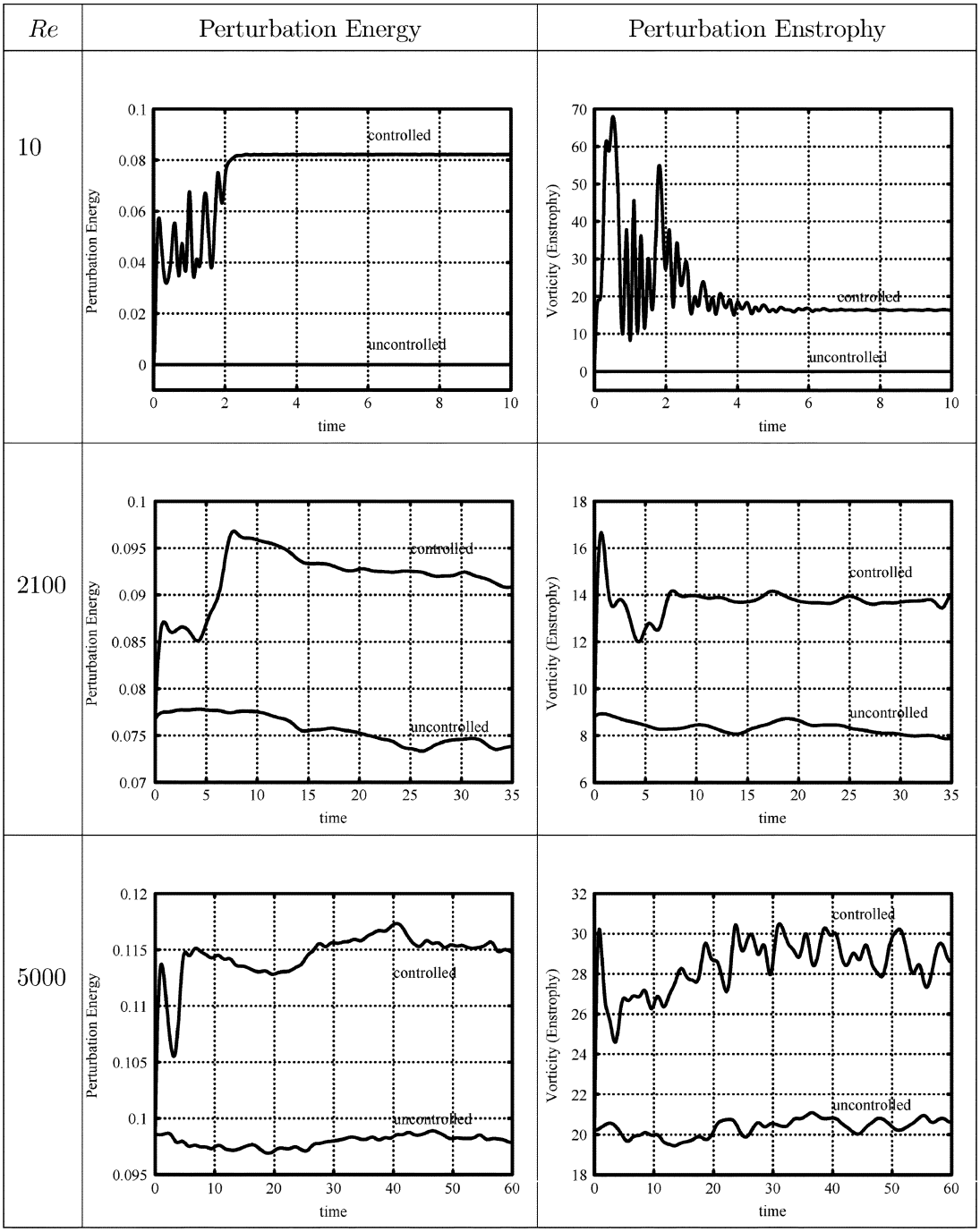

Fig. 3. Perturbation energy and perturbation enstrophy.

turbulent (Re $= 5000$) case, we cannot expect dramatic changes, but the increase in the measured quantities would be considered significant in applications. The instantaneous streamwise vorticity along a cross section of the pipe (Fig. 4) also shows some promise for increased mixing with higher values of vorticity and more complex vortex structures in the controlled case than in the uncontrolled case. Vorticity is increased not only near the wall but everywhere in the pipe.

The method we use to quantify and visualize mixing is the tracking of dye in the flow. We consider the problem of mixing of a single fluid (or similar fluids) governed by the stretching and folding of material elements. We introduce passive tracer dye

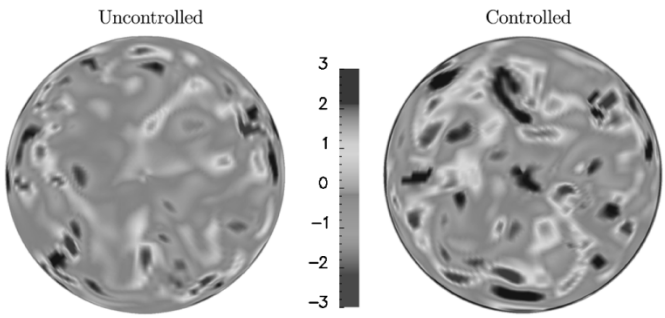

Fig. 4. Streamwise vorticity at Re $= 2100$.

Fig. 5. Initial particle distribution.

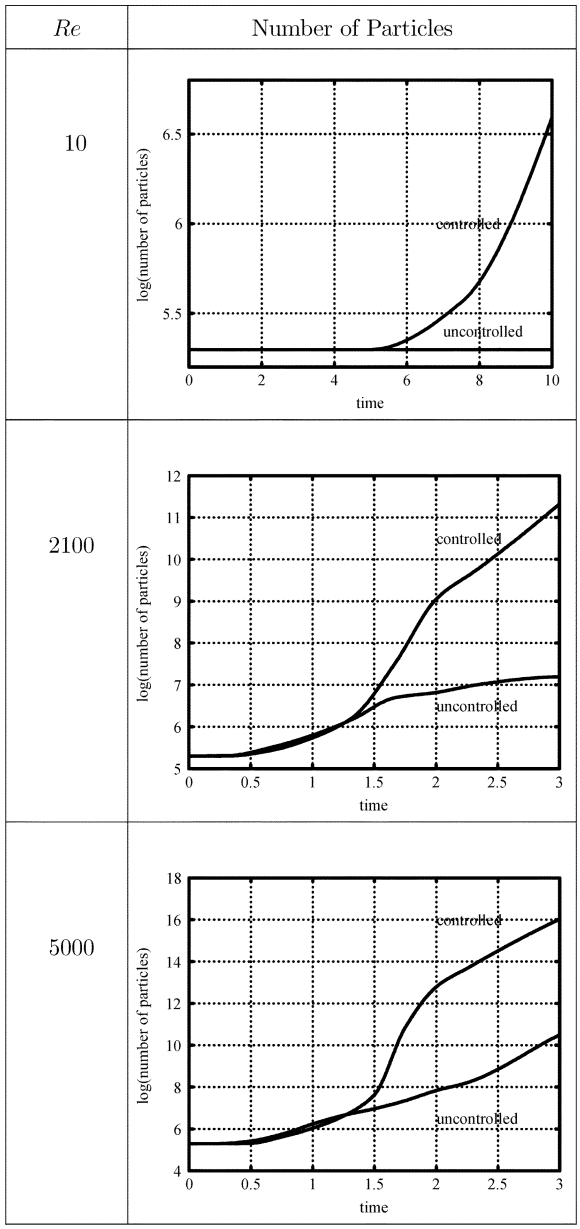

Fig. 6. Length of dye as a function of time.

along the center of the pipe represented by a set of 100 particles (Fig. 5). We trace the position of these particles using a particle-line method [14], [32]. The distance between neighboring particles is kept under 0.1 by introducing new particles to halve the distance if necessary to obtain a connected dye surface at all time. As shown in Fig. 6, the number of particles, that is, the length of the dye, increases in the controlled case at a much higher rate than in the uncontrolled case. Adding particles is not feasible computationally for an extended period of time. We stopped adding particles when their number reached two million ($t = 4$ in the controlled case and $t = 8$ in the uncontrolled case), but we continued tracing them. Fig. 7 shows the distribution of particles inside the pipe. In the controlled case, we obtain more uniform particle distribution even for smaller time.

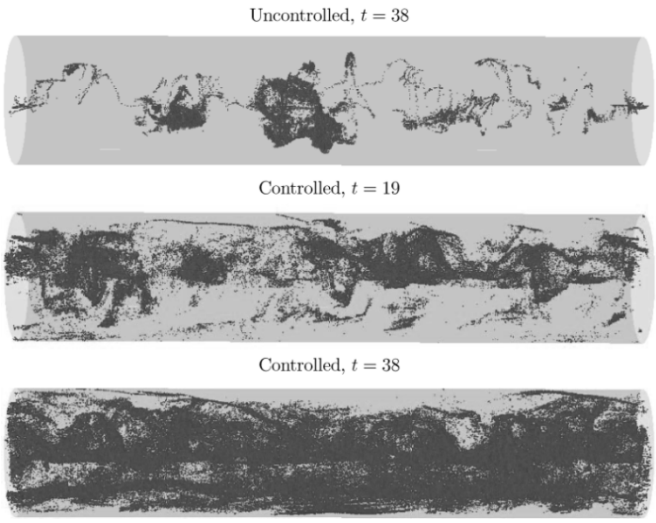

Fig. 7. Particle distribution Re $= 2100$.

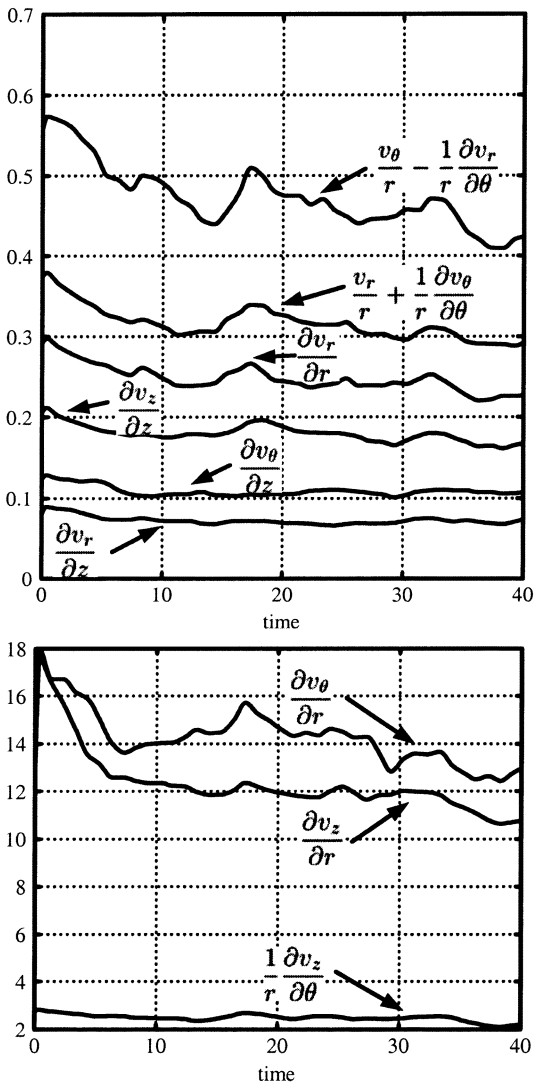

Fig. 8. Parts of functional $m(\mathbf{w})$ for Re $= 2100$.

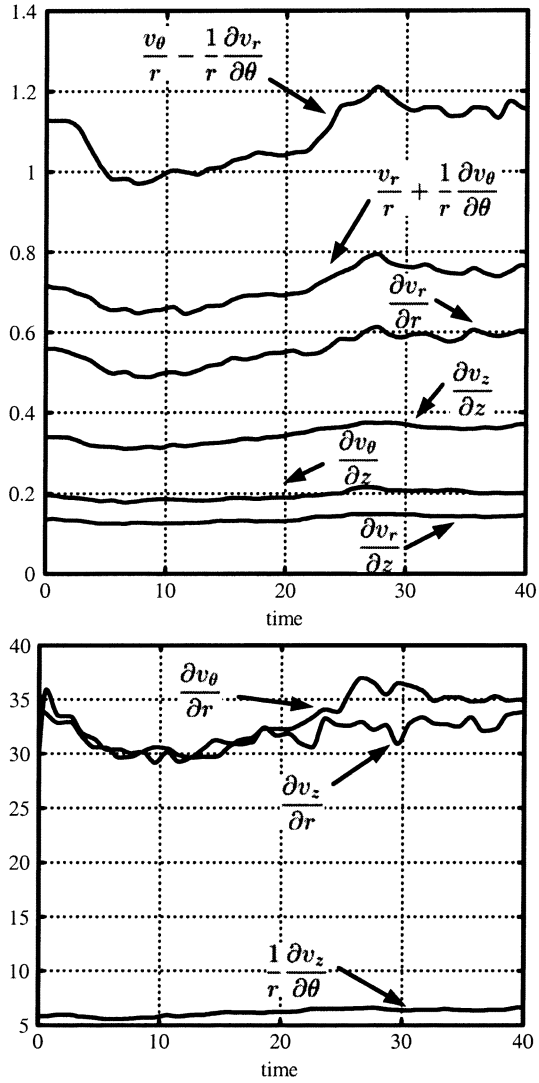

Fig. 9. Parts of functional $m(\mathbf{w})$ for Re $= 5000$.

We compare the nine different parts of functional $m(\mathbf{w})$ for different Reynolds numbers in Figs. 8 –10. In these figures, we omit the integral signs as well as the square signs in order to simplify notations. In all the cases, the terms can be divided into two groups: one dominant group and another group with terms more than a magnitude smaller.

We start the comparison with the large Reynolds number cases Re $= 2100$ and Re $= 5000$ (see Figs. 8 and 9), because they have similar features. In both of these cases, there are two parts that are significantly larger than the rest: the parts containing $(\partial v_\theta)/(\partial r)$ and $(\partial v_z)/(\partial r)$. The next large term corresponds to the expression $(1/r)(\partial v_z)/(\partial \theta)$ and it is four to six times smaller than the two largest terms. The rest of the terms are about 30 to 200 times smaller than the two largest terms.

For Reynolds number Re $= 10$ some of the terms have large values and their behavior is chaotic for the initial transient time $t \in [0, 6]$. We only make comparison for larger time in Fig. 10. The dominant terms are the ones containing $(\partial v_r)/(\partial r), (v_\theta)/(r) - (1/r)(\partial v_r)/(\partial \theta), (v_r)/(r) + (1/r)(\partial v_\theta)/(\partial \theta)$, and $(\partial v_z)/(\partial r)$. Only the last one of these

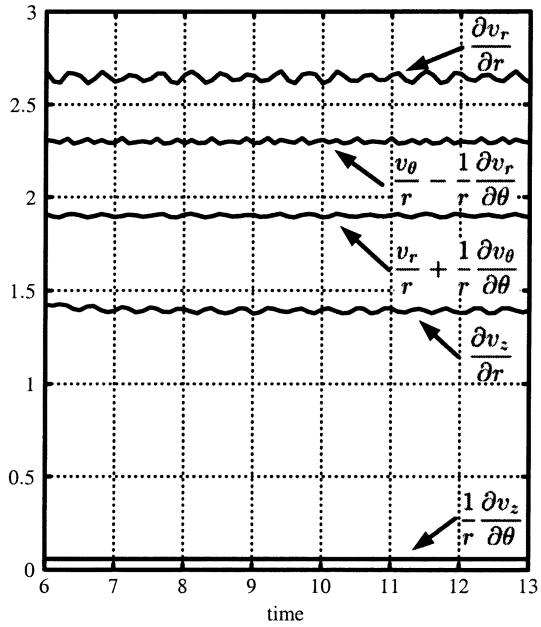

Fig. 10. Parts of functional $m(\mathbf{w})$ for Re $= 10$.

terms, the terms containing $(\partial v_z)/(\partial r)$ belongs to the dominant group for larger Reynolds numbers. The term containing $(1/r)(\partial v_z)/(\partial \theta)$ is one magnitude smaller than these four dominant terms. The rest of the terms are all four magnitude smaller and are omitted from the figure.

C. Measure of Control Effort

In the previous subsection our numerical simulations show significant mixing results with our feedback boundary control law. This control law is optimal with respect to the cost functional (20). In this section, we measure how big the control effort is relative to natural quantities in the pipe flow.

Fig. 11 compares the natural pressure power $(\int_0^{2\pi} \int_0^1 p v_z r \, dr \, d\theta)$ that propels the flow through the channel to the power of the control actuation $(\int_0^{2\pi} \int_0^L p u \, dz \, d\theta)$. The actuation power is four magnitude smaller than the natural pressure power for all three Reynolds numbers. The negative sign of the actuation power shows that the actuation acts against high pressure on the wall by blowing inward the pipe.

We compare the pipe flux $(\int_0^{2\pi} \int_0^1 v_z \, dr \, d\theta)$ and the actuation flux $(\int_0^{2\pi} \int_0^L |u| \, dr \, d\theta)$ with the help of Fig. 12. As we stated earlier, the pipe flux is set to constant one per unit span. The actuation flux is one quarter of the pipe flux for Re $= 10$ and about one eighth of the pipe flux for Re $= 2100$ and Re $=$ 5000. The maximum velocity at the wall is 10^{-3} for Re $= 10$ and 5×10^{-4} for Re $= 2100$ and for Re $= 5000$.

D. Actuator Distribution and Bandwidth for Re = 2100

Fig. 13 shows the instantaneous pressure field in a cross section of the pipe along with the boundary velocity that is magnified 500 times for visualization. The control "blows in" when wall pressure is high and "sucks out" when wall pressure is low. Spatial changes in the control velocity are smooth and small, promising that low number of actuators will suffice in practice.

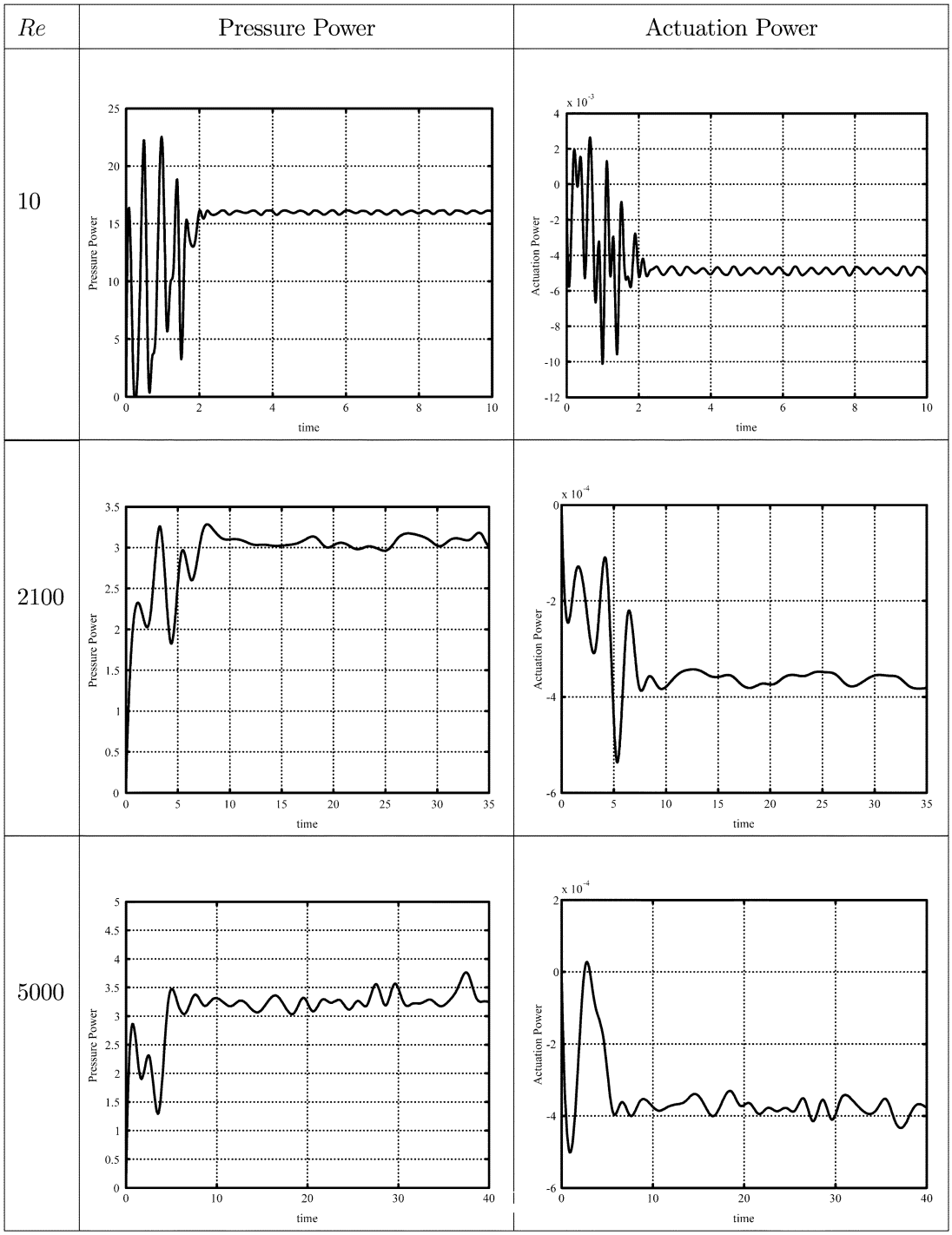

Fig. 11. Pressure power and actuation power.

In order to investigate the density and bandwidth of sensors and actuators needed we calculate the power spectral densities of the control. The spectral plots alongside with the original signals are shown in Fig. 14. Fig. 14(a) and (b) shows that only about 10–15 actuators/sensors are needed along the pipe length. Similarly, in the angular direction [see Fig. 14(c) and (d)] we need at most 15–20 actuators/sensors. That results in approximately 200 micro-actuators/sensors for the whole pipe surface. The time-frequency analysis [Fig. 14(e) and (f)] shows a bandwidth required for sensing/actuation of only 1.5 Hz.

IX. Concluding Remarks

We have shown that mixing in 3-D pipe flow is considerably enhanced by applying small amounts of blowing and suction across the pipe wall. With the L_2-norm of first-order spatial derivatives of the flow perturbations as a measure of mixing, we have designed a Lyapunov based control law that maximizes this measure, while at the same time minimizing the control effort and the sensing effort. The penalty on sensing resulted in a static *output*-feedback control law (rather than full-state feedback). A lower bound on the gain from the control effort

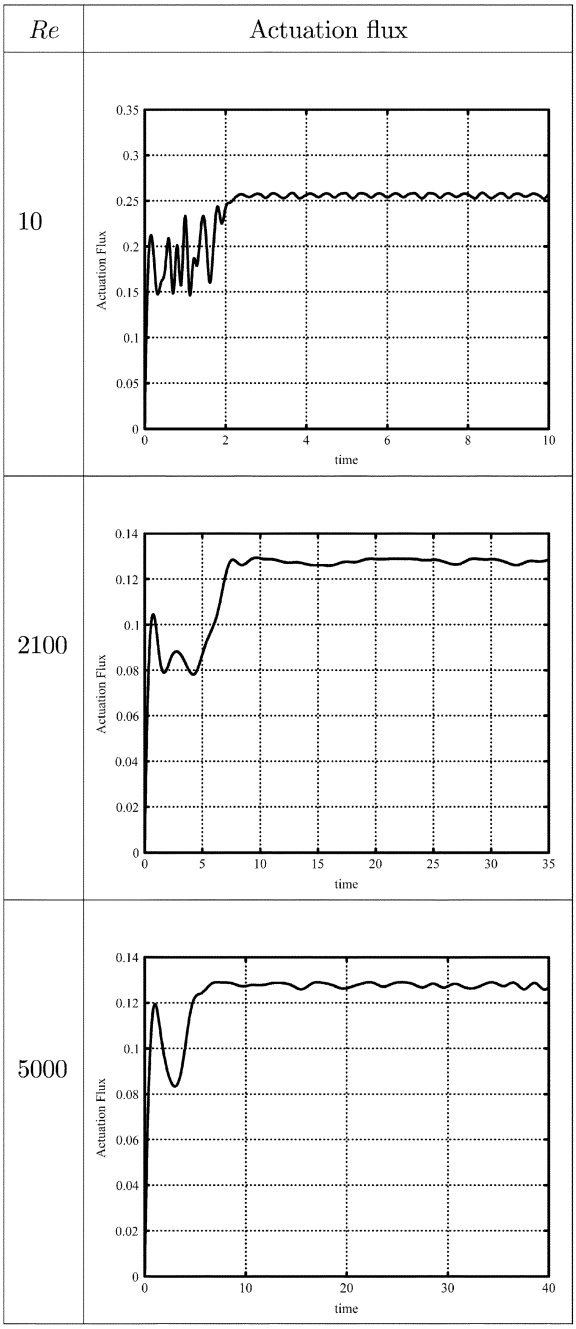

Fig. 12. Actuation flux.

to the mixing measure was also derived. For the open-loop system, input–output-to-state-stability properties were established, which show a form of detectability of mixing in the interior of the pipe from the chosen outputs on the wall.

The effectiveness of the optimal control in achieving mixing enhancement was demonstrated in numerical simulations of the 3-D pipe flow at Reynolds numbers 10, 2100, and 5000. Massless particles placed into the flow, simulating passive tracer dye, indicated considerable mixing enhancement as a result of the control. Simulation results also showed that the spatial changes in the control velocity were smooth and small, promising that a low number of actuators will suffice in practice.

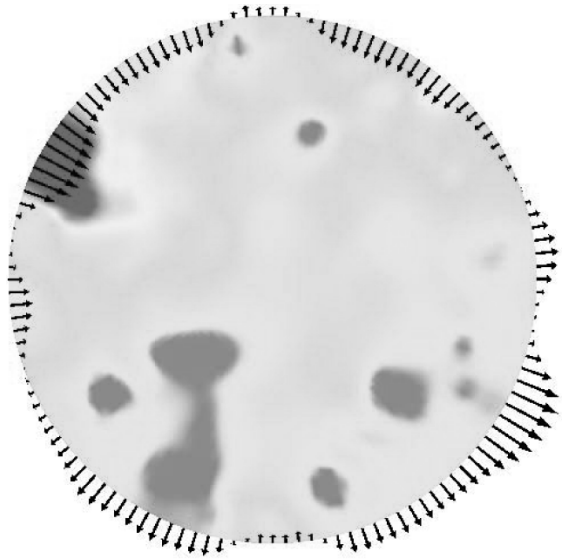

Fig. 13. Instantaneous pressure field with controlled velocity (magnified) in a cross section of the pipe Re $= 2100$.

APPENDIX

A. Proof of Lemma 1

The time derivative of $E(\mathbf{w})$ along trajectories of (5)–(6) is

$$\dot{E}(\mathbf{w}) = \int_\Omega \frac{\partial \mathbf{w}}{\partial t} \cdot \mathbf{w}\, dV \tag{45}$$

so inserting (5) we have

$$\begin{aligned}\dot{E}(\mathbf{w}) = &- \int_\Omega (\mathbf{w}\cdot\nabla)\mathbf{w}\cdot\mathbf{w}\, dV \\ &- \int_\Omega [(\mathbf{w}\cdot\nabla)\bar{\mathbf{W}} + (\bar{\mathbf{W}}\cdot\nabla)\mathbf{w}]\cdot\mathbf{w}\, dV \\ &- \int_\Omega \nabla p\cdot\mathbf{w}\, dV + \frac{1}{\mathrm{Re}}\int_\Omega \Delta\mathbf{w}\cdot\mathbf{w}\, dV. \end{aligned} \tag{46}$$

We will now integrate term by term using the divergence theorem of Gauss, and the following three formulas from vector differential calculus (can be found in any book on calculus)[1]

$$\mathrm{div}(f\mathbf{w}) = \mathbf{w}\cdot\nabla f \tag{47}$$

$$\Delta(fg) = g\Delta f + 2\nabla f\cdot\nabla g + f\Delta g \tag{48}$$

$$\Delta f = \mathrm{div}(\nabla f). \tag{49}$$

a) *Convective term*

$$\begin{aligned} -\int_\Omega (\mathbf{w}\cdot\nabla)\mathbf{w}\cdot\mathbf{w}\, dV &= -\frac{1}{2}\int_\Omega \nabla(\mathbf{w}\cdot\mathbf{w})\mathbf{w}\, dV \\ &= -\frac{1}{2}\int_\Omega \mathrm{div}((\mathbf{w}\cdot\mathbf{w})\mathbf{w})\, dV \end{aligned} \tag{50}$$

so, by the divergence theorem of Gauss, we get

$$-\int_\Omega (\mathbf{w}\cdot\nabla)\mathbf{w}\cdot\mathbf{w}\, dV = -\frac{1}{2}\int_{\partial\Omega} [(\mathbf{w}\cdot\mathbf{w})\mathbf{w}]\cdot\mathbf{n}\, dA. \tag{51}$$

[1]In (47), we have used (6).

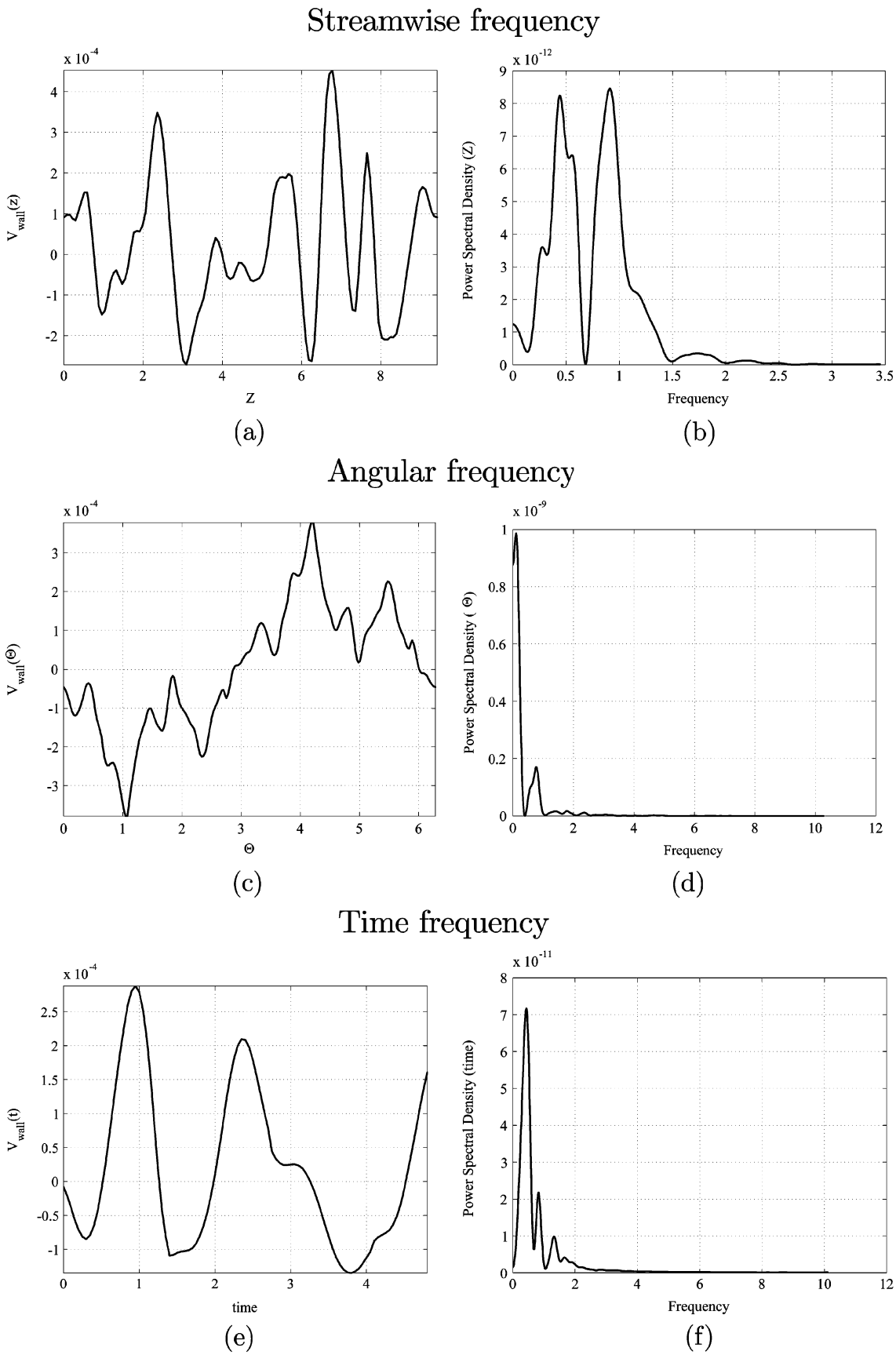

Fig. 14. Spectral analysis of the control Re = 2100. (a) Control signal. (b) Power spectral density. (c) Control signal. (d) Power spectral density. (e) Control signal. (f) Power spectral density.

$\mathbf{w}\cdot\mathbf{n} = u$ on $\partial\Omega$, so the integrand in the last integral of (51) is simply u^3. Since u has the form (10), we have for odd n

$$\int_0^{2\pi} u^n d\theta = \int_{-\pi}^{0} u^n d\theta + \int_0^{\pi} u^n d\theta = -\int_{-\pi}^{0} u^n(-\theta,z,t)\,d\theta + \int_0^{\pi} u^n(\theta,z,t)\,d\theta$$

and by a change of variables in the first integral ($\theta^* = -\theta$), we get

$$\int_0^{2\pi} u^n d\theta = -\int_0^{\pi} u^n(\theta^*,z,t)\,d\theta^* + \int_0^{\pi} u^n(\theta,z,t)\,d\theta = 0.$$

So we obtain

$$-\int_\Omega (\mathbf{w}\cdot\nabla)\mathbf{w}\cdot\mathbf{w}\,dV = 0. \tag{52}$$

b) *Crossterm*

$$-\int_\Omega \left[(\mathbf{w}\cdot\nabla)\bar{\mathbf{W}} + (\bar{\mathbf{W}}\cdot\nabla)\,\mathbf{w}\right]\cdot\mathbf{w}\,dV = -\Gamma(\mathbf{w}) \tag{53}$$

by definition of $\Gamma(\mathbf{w})$.

c) *Pressure term*

$$-\int_\Omega \nabla p\cdot\mathbf{w}\,dV = -\int_\Omega \operatorname{div}(p\mathbf{w})\,dV \tag{54}$$

so by the divergence theorem of Gauss, and the fact that $\mathbf{w}\cdot\mathbf{n} = u$ on $\partial\Omega$

$$-\int_\Omega \nabla p\cdot\mathbf{w}\,dV = -\int_{\partial\Omega} pu\,dA. \tag{55}$$

From (10) and (11) we have

$$\begin{aligned}\int_0^{2\pi}[up]_{r=1}\,d\theta &= \int_0^{\pi}[up]_{r=1}\,d\theta + \int_\pi^{2\pi}[up]_{r=1}\,d\theta\\ &= \int_0^{\pi}[up]_{r=1}\,d\theta\\ &\quad - \int_0^{\pi} u(\theta,z,t)p(1,\theta+\pi,z,t)\,d\theta\\ &= \int_0^{\pi} u(\theta,z,t)y\,d\theta\\ &= \frac{1}{2}\int_0^{2\pi} u(\theta,z,t)y\,d\theta\end{aligned} \tag{56}$$

so we obtain

$$-\int_\Omega \nabla p\cdot\mathbf{w}\,dV = -\frac{1}{2}\int_{\partial\Omega} uy\,dA. \tag{57}$$

d) *Dissipation term*

$$\begin{aligned}\frac{1}{\mathrm{Re}}\int_\Omega \Delta\mathbf{w}\cdot\mathbf{w}\,dV &= \frac{1}{\mathrm{Re}}\int_\Omega (\Delta w_i)w_i\,dV\\ &= \frac{1}{\mathrm{Re}}\int_\Omega [\Delta(w_iw_i) - 2\nabla w_i\cdot\nabla w_i - w_i(\Delta w_i)]\,dV\end{aligned} \tag{58}$$

where we have adopted the Einstein summation notation. From (58) we get

$$\frac{1}{\mathrm{Re}}\int_\Omega \Delta\mathbf{w}\cdot\mathbf{w}\,dV = \frac{1}{2\mathrm{Re}}\int_\Omega \Delta(w_iw_i)\,dV - \frac{1}{\mathrm{Re}}\int_\Omega |\nabla\mathbf{w}|^2\,dV. \tag{59}$$

The integrand of the first integral on the right hand side of (59) can be written as $\operatorname{div}(\nabla(|\mathbf{w}|^2))$, so by the divergence theorem of Gauss, we get

$$\int_\Omega \Delta(w_iw_i)\,dV = \int_{\partial\Omega} (\nabla|\mathbf{w}|^2)\cdot\mathbf{n}\,dA. \tag{60}$$

Since the control is wall-normal, the integrand on the right hand side of (60) reduces to

$$2v_r\frac{\partial v_r}{\partial r}. \tag{61}$$

We now note from incompressibility (6), which in cylindrical coordinates reads

$$\frac{1}{r}\frac{\partial}{\partial r}(rv_r) + \frac{1}{r}\frac{\partial v_\theta}{\partial\theta} + \frac{\partial v_z}{\partial z} = 0 \tag{62}$$

that

$$\frac{\partial v_r}{\partial r}(1,\theta,z,t) = -v_r(1,\theta,z,t). \tag{63}$$

Thus, by inserting (63) into (61), (61) into (60), and (60) into (59), we obtain

$$\frac{1}{\mathrm{Re}}\int_\Omega \Delta\mathbf{w}\cdot\mathbf{w}\,dV = -\frac{1}{\mathrm{Re}}\int_\Omega |\nabla\mathbf{w}|^2\,dV - \frac{1}{\mathrm{Re}}\int_{\partial\Omega} u^2\,dA. \tag{64}$$

Substituting the terms (52), (53), (57), and (64) into (46) yields (16). ■

B. Proof of Lemma 2

Using cylindrical coordinates, we have that

$$\Gamma(\mathbf{w}) = \int_0^L\int_0^{2\pi}\int_\varepsilon^1 v_zv_r\frac{\partial\bar{V}_z}{\partial r}r\,dr\,d\theta\,dz. \tag{65}$$

Since $\sup_\Omega |(\partial \bar{V}_z)/(\partial r)| = 2$, we have

$$\int_0^L \int_0^{2\pi} \int_\varepsilon^1 v_z v_r \frac{\partial \bar{V}_z}{\partial r} r\, dr\, d\theta\, dz \le 2 \int_0^L \int_0^{2\pi} \int_\varepsilon^1 |v_z||v_r| r\, dr \le a \int_0^L \int_0^{2\pi} \int_\varepsilon^1 v_r^2 r\, dr\, d\theta\, dz + \frac{1}{a} \int_0^L \int_0^{2\pi} \int_\varepsilon^1 v_z^2 r\, dr\, d\theta\, dz. \quad (66)$$

We write

$$v_r(r,\theta,z,t) = u - \int_r^1 \frac{\partial v_r}{\partial r}\, dr$$

so that

$$v_r^2(r,\theta,z,t) = \left(u - \int_r^1 \frac{\partial v_r}{\partial r}\, dr \right)^2 \le (1+b)u^2 + \left(1 + \frac{1}{b}\right) \left(\int_r^1 \frac{\partial v_r}{\partial r}\, dr \right)^2.$$

By the Schwartz inequality

$$\left(\int_r^1 \frac{1}{\sqrt{r}} \sqrt{r} \frac{\partial v_r}{\partial r}\, dr \right)^2 \le -\ln r \int_r^1 r \left(\frac{\partial v_r}{\partial r} \right)^2 dr$$

so we have that

$$r v_r^2(r,\theta,z,t) \le (1+b) r u^2 - \left(1 + \frac{1}{b}\right) r \ln r \int_\varepsilon^1 r \left(\frac{\partial v_r}{\partial r} \right)^2 dr$$

where we have set $r = \varepsilon$ in the lower integral limit. We now get

$$\int_0^L \int_0^{2\pi} \int_\varepsilon^1 v_r^2 r\, dr\, d\theta\, dz \le \int_0^L \int_0^{2\pi} \int_\varepsilon^1 \left((1+b) r u^2 - \left(1 + \frac{1}{b}\right) r \ln r \int_\varepsilon^1 r \left(\frac{\partial v_r}{\partial r} \right)^2 dr \right) dr\, d\theta\, dz = \frac{1}{2}(1-\varepsilon^2)(1+b) \int_0^L \int_0^{2\pi} u^2\, d\theta\, dz + \frac{1}{4}\left(1 - \varepsilon^2 + 2\varepsilon^2 \ln \varepsilon\right) \left(1 + \frac{1}{b}\right) \times \int_0^L \int_0^{2\pi} \int_\varepsilon^1 r \left(\frac{\partial v_r}{\partial r} \right)^2 dr\, d\theta\, dz. \quad (67)$$

For v_z, we have

$$v_z(r,\theta,z,t) = -\int_r^1 \frac{\partial v_z}{\partial r}\, dr$$

so we get

$$v_z^2(r,\theta,z,t) = \left(\int_r^1 \frac{1}{\sqrt{r}} \sqrt{r} \frac{\partial v_z}{\partial r} dr \right)^2 \le -\ln r \int_r^1 r \left(\frac{\partial v_z}{\partial r} \right)^2 dr$$

and, finally

$$\int_0^L \int_0^{2\pi} \int_\varepsilon^1 v_z^2\, r\, dr\, d\theta\, dz \le \int_0^L \int_0^{2\pi} \int_\varepsilon^1 -r \ln r \int_\varepsilon^1 r \left(\frac{\partial v_z}{\partial r} \right)^2 dr\, dr\, d\theta\, dz = \frac{1}{4}\left(1 - \varepsilon^2 + 2\varepsilon^2 \ln \varepsilon\right) \int_0^L \int_0^{2\pi} \int_\varepsilon^1 r \left(\frac{\partial v_z}{\partial r} \right)^2 dr\, d\theta\, dz. \quad (68)$$

Inserting (67) and (68) into (66), and letting $\varepsilon \to 0$, yield

$$\int_0^L \int_0^{2\pi} \int_0^1 v_z v_r \frac{\partial \bar{V}_z}{\partial r} r\, dr\, d\theta\, dz \le \frac{a}{4}\left(1 + \frac{1}{b}\right) \int_0^L \int_0^{2\pi} \int_0^1 \left(\frac{\partial v_r}{\partial r} \right)^2 r\, dr\, d\theta\, dz + \frac{1}{4a} \int_0^L \int_0^{2\pi} \int_0^1 \left(\frac{\partial v_z}{\partial r} \right)^2 r\, dr\, d\theta\, dz. \quad (69)$$

(18) now follows from (65), (69), and (15). ■

ACKNOWLEDGMENT

The authors would like to thank C. Pierce for providing the code for the uncontrolled case.

REFERENCES

[1] O. M. Aamo, M. Krstić, and T. R. Bewley, "Control of mixing by boundary feedback in 2-D channel flow," *Automatica*, vol. 39, no. 9, pp. 1597–1606, 2003.

[2] K. Akselvoll and P. Moin, "An efficient method for temporal integration of the Navier-Stokes equations in confined axisymmetric geometry," *J. Computat. Phys.*, vol. 125, pp. 454–463, 1996.

[3] A. M. Annaswamy and A. F. Ghoniem, "Active control in combustion systems," *IEEE Control Syst. Mag.*, vol. 15, no. 6, pp. 49–63, Dec. 1995.

[4] H. Aref, "Stirring by chaotic advection," *J. Fluid Mech.*, vol. 143, pp. 1–21, 1984.

[5] W.-L. Chien, H. Rising, and J. M. Ottino, "Laminar mixing and chaotic mixing in several cavity flows," *J. Fluid Mech.*, vol. 170, pp. 355–377, 1986.

[6] D. D'Alessandro, M. Dahleh, and I. Mezić, "Control of fluid mixing using entropy methods," in *Proc. Amer. Control Conf.*, Philadelphia, PA, 1998.
[7] ——, "Control of mixing in fluid flow: A maximum entropy approach," *IEEE Trans. Autom. Control*, vol. 44, no. 10, pp. 1852–1863, Oct. 1999.
[8] A. F. Ghoniem and K. K. Ng, "Numerical study of the dynamics of a forced shear layer," *Phys. Fluids*, vol. 30, no. 3, pp. 706–721, 1987.
[9] G. Haller and A. C. Poje, "Finite time transport in aperiodic flows," *Physica D*, vol. 119, pp. 352–380, 1998.
[10] G. Haller, "Finding finite-time invariant manifolds in two-dimensional velocity fields," *Chaos*, vol. 10, no. 1, 2000.
[11] G. Haller and G. Yuan, "Lagrangian coherent structures and mixing in two-dimensional turbulence," *Physica D*, vol. 147, pp. 352–370, 2000.
[12] G. Haller, "Distinguished material surfaces and coherent structures in three-dimensional fluid flows," *Physica D*, vol. 149, pp. 248–277, 2001.
[13] D. V. Khakhar, H. Rising, and J. M. Ottino, "Analysis of chaotic mixing in two model systems," *J. Fluid Mech.*, vol. 172, pp. 419–451, 1986.
[14] T. S. Krasnopolskaya, V. V. Meleshko, G. W. M. Peters, and H. E. H. Meier, "Mixing in stokes flow in an annular wedge cavity," *Eur. J. Mech. B/Fluids*, vol. 18, pp. 793–822, 1999.
[15] M. Krichman, E. D. Sontag, and Y. Wang, "Input-output-to-state stability," in *SIAM J. Control Optim.*, vol. 39, 2001, pp. 1874–1928.
[16] M. Krstić, I. Kanellakopoulos, and P. Kokotović, *Nonlinear and Adaptive Control Design*. New York: Wiley, 1995.
[17] C. W. Leong and J. M. Ottino, "Experiments on mixing due to chaotic advection in a cavity," *J. Fluid Mech.*, vol. 209, pp. 463–499, 1989.
[18] N. Malhotra, I. Mezić, and S. Wiggins, "Patchiness: A new diagnostic for Lagrangian trajectory analysis in time-dependent fluid flows," *Int. J. Bifurcation Chaos*, vol. 8, no. 6, pp. 1053–1093, 1998.
[19] I. Mezić, "On geometrical and statistical properties of dynamical systems: Theory and applications," Ph.D. dissertation, California Inst. Tech., Pasadena, 1994.
[20] I. Mezić and S. Wiggins, "A method for visualization of invariant sets of dynamical systems based on the ergodic partition," *Chaos*, vol. 9, no. 1, pp. 213–218, 1999.
[21] I. Mezić, "Nonlinear dynamics and ergodic theory methods in control of fluid flows: Theory and applications," in *Proc. 2001 AFOSR Workshop Dynamics Control*, 2001.
[22] P. D. Miller, C. K. R. T. Jones, A. M. Rogerson, and L. J. Pratt, "Quantifying transport in numerically generated velocity fields," *Physica D*, vol. 110, pp. 105–122, 1997.
[23] B. R. Noack, I. Mezić, and A. Banaszuk, "Controlling vortex motion and chaotic advection," in *Proc. 39th IEEE Conf. Decision Control*, Sydney, Australia, Dec. 11–15, 2000, pp. 1716–1723.
[24] J. M. Ottino, *The Kinematics of Mixing: Stretching, Chaos, and Transport*. Cambridge, U.K.: Cambridge Univ. Press, 1989.
[25] ——, "Mixing, chaotic advection, and turbulence," *Annu. Rev. Fluid Mech.*, vol. 22, pp. 207–253, 1990.
[26] A. C. Poje, G. Haller, and I. Mezić, "The geometry and statistics of mixing in aperiodic flows," *Phys. Fluids*, vol. 11, no. 10, 1999.
[27] A. C. Poje and G. Haller, "Geometry of cross-stream mixing in a double-gyre ocean model," *J. Phys. Oceanogr.*, vol. 29, pp. 1469–1665, 1999.
[28] V. Rom-Kedar, A. Leonard, and S. Wiggins, "An analytical study of transport, mixing, and chaos in an unsteady vortical flow," *J. Fluid Mech.*, vol. 214, pp. 347–394, 1990.
[29] E. D. Sontag and Y. Wang, "Output-to-state stability and detectability of nonlinear systems," *Syst. Control Lett.*, vol. 29, pp. 279–290, 1997.
[30] E. D. Sontag, "Comments on integral variants of ISS," *Syst. Control Lett.*, vol. 34, pp. 93–100, 1998.
[31] P. D. Swanson and J. M. Ottino, "A comparative computational and experimental study of chaotic mixing of viscous fluids," *J. Fluid Mech.*, vol. 213, pp. 227–249, 1990.
[32] A. A. Ten, Y. Y. Podladchikov, D. A. Yuan, T. B. Larsen, and A. V. Malevsky, "Comparison of mixing properties in convection with the particle-line method," *Geophys. Res. Lett.*, vol. 25, pp. 3205–3208, 1998.

Andras Balogh received the B.S. degree in mathematics from the University of Szeged, Hungary, in 1989, the M.S. degree in applied mathematics from the University of Texas, Dallas, in 1994, and the Ph.D. degree in mathematics from Texas Tech. University, Lubbock, in 1997.

He was a Visiting Assistant Professor at Idaho State University, Pocatello, from 1997 to 1998 and an Assistant Project Scientist in the Department of Mechanical and Aerospace Engineering, University of California, San Diego, La Jolla, from 1998 to 2002. He is currently an Assistant Professor of Mathematics in the Department of Mathematics, University of Texas-Pan American, Edinburg. His research interests include nonlinear evolution equations, control of distributed parameter systems and computational mathematics.

Ole Morten Aamo recieved the M.S. and Ph.D. degrees in engineering cybernetics from the Norwegian University of Science and Technology (NTNU), Trondheim, in 1992 and 2002, respectively.

From 2002 to 2003, he was a Postdoctoral Fellow at the Marine Technology Department, NTNU, and now holds a Postdoctoral position at the Engineering Cybernetics Department. He is a coauthor of the book *Flow Control by Feedback* (New York: Springer-Verlag, 2002). His research interests include control of distributed parameter systems with special emphasis on fluid flows.

Miroslav Krstić (F'01) received the Ph.D. degree in electrical engineering from the University of California, Santa Barbara (UCSB), under the advisement of Petar Kokotovic.

He is a Professor and Vice Chair in the Department of Mechanical and Aerospace Egineering at University of California at San Diego (UCSD), La Jolla. Prior to moving to UCSD, he was an Assistant Professor in the Department of Mechanical Engineering and the Institute of Systems Research, the University of Maryland, College Park, from 1995 to 1997. He is a coauthor of the books *Nonlinear and Adaptive Control Design* (New York: Wiley, 1995), *Stabilization of Nonlinear Uncertain Systems* (New York: Springer-Verlag, 1998), *Flow Control by Feedback* (New York: Springer-Verlag, 2002), and *Real Time Optimization by Extremum Seeking Control* (New York: Wiley, 2003). He is a coauthor of two patents on control of aeroengine compressors and combustors. His research interests include nonlinear, adaptive, robust, and stochastic control theory for finite-dimensional and distributed parameter systems, and applications to fluid flows and fusion.

Dr. Krstic received the UCSB Best Dissertation Award, the National Science Foundation Career Award, the Office of Naval Research Young Investigator Award, the Presidential Early Career Award for Scientists and Engineers (PECASE), the George S. Axelby Outstanding Paper Award of the IEEE TRANSACTIONS ON AUTOMATIC CONTROL, and the O. Hugo Schuck Award for the Best Paper at the American Control Conference. He has served as Associate Editor for the IEEE TRANSACTIONS ON AUTOMATIC CONTROL, the *International Journal of Adaptive Control and Signal Processing*, *Systems and Control Letters*, and the *Journal for Dynamics of Continuous, Discrete, and Impulsive Systems*. He is a Vice President for Technical Activities and a Member of the Board of Governors of the IEEE Control Systems Society.